RSC Advances

PAPER

View Article Online
View Journal | View Issue

Cite this: *RSC Adv.*, 2016, **6**, 58823

Enhanced electrochemical performance of phosphorus incorporated carbon nanofibers by the spin-on dopant method†

Dong-Yo Sin, Il-Kyu Park* and Hyo-Jin Ahn*

Received 14th March 2016
Accepted 10th June 2016

DOI: 10.1039/c6ra06782d

www.rsc.org/advances

Phosphorus-incorporated carbon nanofibers (CNFs) were successfully fabricated by using electrospinning and spin-on dopant (SOD) procedures together for electrochemical capacitors (ECs). Microstructural and chemical investigations indicated that phosphorus was uniformly incorporated into the CNFs without any impurities or alloys by using an SOD treatment. The specific surface area of the SOD-treated CNFs increased by over 1.47 times when compared to that of conventional CNFs due to an increase in the total pore volume. In addition, the SOD-treated CNFs contained many beneficial functional groups such as phosphate and hydroxyl groups. ECs, fabricated from SOD-treated CNFs as electrodes, showed enhanced electrochemical performance such as high capacitance (up to 188 F g^{-1}), good high-rate performance with a capacitance retention of 84%, an excellent energy density (17.2–23.5 W h kg^{-1} in a power density ranging from 360 to 4680 W kg^{-1}), and an excellent cycle stability (86% up to 1000 cycles). These enhancements were attributed to the beneficial effects of the SOD method applied to the CNFs to enlarge the surface area and provide many functional groups.

1. Introduction

Recently, carbon-based materials such as graphite, graphene, carbon nanotubes, and carbon nanofibers (CNFs) have received considerable interest owing to their potential applications in a variety of fields such as photovoltaic devices, environmental applications, and electrical energy-storage devices.[1–4] Notably, these carbon-based materials have been investigated for their potential application as electrode materials for energy-storage devices such as electrochemical capacitors (ECs), lithium-ion batteries, and fuel cells (FCs) because of their low cost, eco-friendliness, high electric conductivity, and thermal/chemical stabilities.[5–8] Among them, CNF structures are of considerable interest because of their potential in providing superior properties for EC applications. This is due to their high specific surface area, low electrical resistivity, thermal/chemical stability, and highly efficient electron transport owing to their one-dimensional nanostructure.[9–11] However, the use of CNFs in EC applications has been limited due to a lower charge-storage capability when compared to the theoretically expected results.[12–14] Therefore, to overcome the limited charge-storage capability of CNFs, various methods have been developed by many research groups. These methods include: controlling the surface morphology, enlarging the specific surface area, and forming various functional groups by incorporating elemental phosphorus, boron, or nitrogen elements.[15–19] In particular, the formation of functional groups on CNFs has been known to significantly enhance the charge-storage capability of ECs by increasing the ionic polarization and wettability of the electrolyte. Recently, bacterial cellulose-derived nitrogen-doped CNFs exhibited a specific capacitance of 254.64 F g^{-1} at a current density of 1.0 A g^{-1}, and an excellent high-rate performance at a current density of 10 A g^{-1} in a 1.0 M Na_2SO_4 aqueous electrolyte.[20] Also, boron-doped mesoporous carbon, synthesized from boric acid, exhibited a specific capacitance of 0.31 F m^{-2} in a 6 M KOH aqueous electrolyte.[21] Furthermore, P-doped graphene, synthesized from phosphoric acid, exhibited a specific capacitance of 115 F g^{-1} at a current density of 0.05 A g^{-1} with a high energy density of 11.64 W h kg^{-1} and a high power density up to 831 W kg^{-1}.[22] In this way, dopants incorporated into carbon-based nanostructures by various methods can improve the performances of ECs. However, these reported methods are based on wet chemical methods that have many detrimental effects. These include difficulties in their synthetic process and incorporation of unwanted impurities. In this study, we provide an alternative method based on a dry process, the spin-on dopant (SOD) process, to incorporate CNFs. The SOD method has many advantages such as low cost, simple synthetic process, and low impurity incorporation. Moreover, it shows great versatility in complicated nanostructures, regardless of the surface morphology, because of their low diffusion activation energy and spatial diffusion directions.[23–27]

Department of Materials Science and Engineering, Seoul National University of Science and Technology, Seoul 139-743, South Korea. E-mail: pik@seoultech.ac.kr; hjahn@seoultech.ac.kr; Fax: +82 029736657; Tel: +82 029706622; +82 029706349

† Electronic supplementary information (ESI) available. See DOI: 10.1039/c6ra06782d

2. Experimental details

2.1. Fabrication of phosphorus-incorporated CNFs

Phosphorus-incorporated CNFs were fabricated by combining an electrospinning process with an SOD method, as shown schematically in Fig. 1. CNFs were synthesized using an electrospinning method. In order to synthesis the CNFs, 10 wt% polyacrylonitrile (PAN, $M_w = 1\,300\,000$, Aldrich) was dissolved in *N*,*N*-dimethylformamide (DMF, 99.8%, Aldrich) for 5 h. To maintain a reliable electrospinning condition, the humidity of the spinning atmosphere was maintained at 10%. The feeding rate of the sources, and the distance between the syringe needle and the collector were fixed at 0.03 mL h^{-1} and 15 cm, respectively, with a working voltage of 13 kV from a DC power supply. The CNFs were stabilized and carbonized by thermal treatment in a tube furnace at 280 °C for 2 h in air and at 800 °C for 2 h in N_2 gas (99.999%) atmosphere, respectively. The heating rate during thermal annealing was fixed at 5 °C min^{-1}. An SOD procedure was used to incorporate elemental P into the CNFs. As a source of incorporation for elemental P, the SOD film was prepared on a Si substrate by spin-coating a P-containing dopant solution (Filmtronic P509; mixture of organic solvents, SiO_2, and P_2O_5 compounds; P concentration in the source of 2×10^{21} at per cm^3). Next, the SOD films were placed at a distance of 1 cm above the as-synthesized CNFs to avoid contamination from direct contact with the SOD films. The samples were loaded into a tube furnace and treated with an SOD film in an Ar gas atmosphere at 500 °C and 800 °C for 5 min each. To demonstrate the effect of P incorporation, we prepared conventional CNFs using the above-mentioned procedures. Henceforth, conventional CNFs and SOD-treated CNFs at 500 °C and 800 °C will be referred to as conventional CNFs, CNF-SOD500, and CNF-SOD800, respectively. The electrochemical properties of the CNFs were examined in slurry form by using a symmetric two-electrode system with 6 M KOH solution as the electrolyte. To measure the electrochemical properties, all samples were prepared in the slurry form and mixed with Ketjen black (Mitsubishi Chemical, ECP-600JD) as a conducting material and poly(vinylidenedifluoride) (PVDF, Alfa Aesar) as a binder in a weight ratio of 8 : 1 : 1. NMP (*N*-methyl-2-pyrrolidone) was used as solvent. All sample slurries were coated on a Ni foam electrode (size of 1 cm × 1 cm), and dried in air at 70 °C for 10 h. The mass and thickness of the electrodes were fixed at 10 mg and 0.1 mm, respectively.

2.2. Characterization of phosphorus-incorporated CNFs

Structural investigations for P-incorporated CNFs were performed by field emission scanning electron microscopy (FESEM; Hitachi S-4700), X-ray diffraction (XRD, Rigaku D/Max-2500 diffractometer equipped with a Cu Kα source), and transmission electron microscopy (TEM; JEOL, KBSI Suncheon Center). Elemental mapping of the samples was carried out using a Phillips CM20T/STEM equipped with an energy-dispersive X-ray spectrometer (EDS). The specific surface area of the CNFs was examined by Brunauer–Emmet–Teller analysis (BET, Micromeritics ASAP2010) using N_2 gas at 350 °C. The CNF chemical bonding states were investigated by X-ray photoelectron spectroscopy (XPS; ESCALAB 250 equipped with an Al Kα X-ray source) under a base pressure of 267 nPa. To investigate the electrochemical properties of CNFs, cyclic voltammetry (CV) measurements were recorded on a potentiostat/galvanostat (Autolab PGSTAT302N, FRA32M) in a potential range of 0.0–1.0 V and a scan rate of 10 mV s^{-1}. Galvanostatic charge/discharge measurements were obtained at a current density of 0.2–2.6 A g^{-1} and a voltage range of 0.0–1.0 V, using a battery cycler system (WonA-Tech., WMPG 1000). The cell cycling stability was investigated for a maximum of 1000 cycles at a current density of 1 A g^{-1}.

3. Results and discussion

Fig. 1 shows a schematic illustration of the synthetic steps of SOD-treated CNFs. First, CNFs were synthesized by an

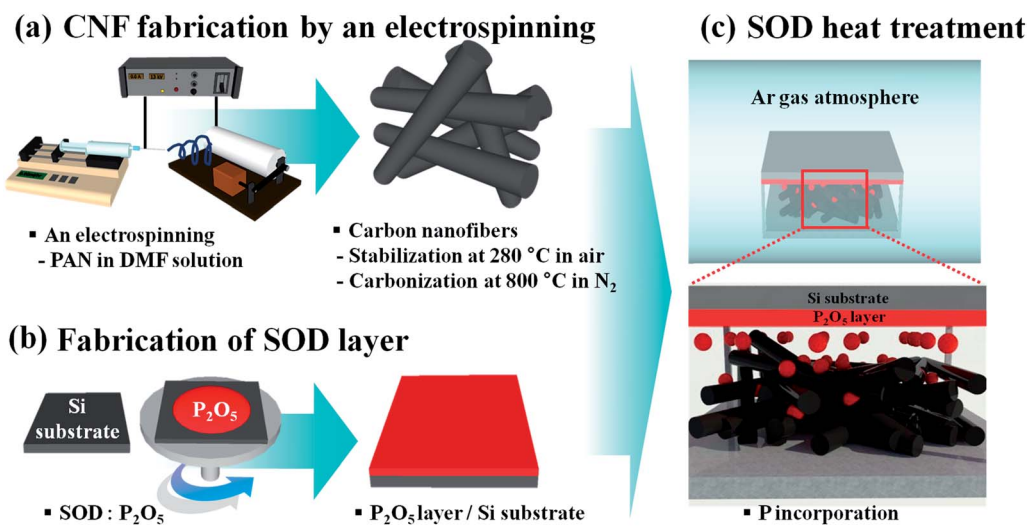

Fig. 1 Schematic of the processing steps for the fabrication of P-incorporated CNFs through an SOD method coupled with an electrospinning method.

electrospinning method using only a PAN polymer. The polymer nanofibers were then stabilized at 280 °C in air, and carbonized at 800 °C in a N_2 atmosphere. Electrospinning is a typical method used in the synthesis of carbon nanofibers owing to its various advantages. These include a simple synthetic process and its facile shape control of nanofibers. Secondly, to incorporate the elemental P, a Si substrate with a P_2O_3 layer coating was prepared by the SOD process. This method is commonly used in the semiconductor manufacturing process. It has excellent advantages such as low cost, a simple synthetic process, low impurity incorporation, and versatile use in complicated nanostructures regardless of the surface morphology. In this study, the SOD process plays a key technological role in the incorporation of P in the prepared CNFs. Finally, the P_2O_5 layer-coated Si substrate was located over the synthesized CNF. Heat treatment was performed at 500 °C and 800 °C for 30 min in Ar atmosphere. We successfully synthesized P-incorporated CNFs using electrospinning and SOD process.

The surface morphology of the CNFs was observed by FESEM. Fig. 2(a–c) show FESEM images of conventional CNFs, CNF-SOD500, and CNF-SOD800, respectively. The surface morphology of the CNFs was smooth and did not change significantly after SOD thermal treatment at various temperatures. The average diameters of the conventional CNFs, CNF-SOD500, and CNF-SOD800 were 228.6, 226.4, and 226 nm, respectively, and showed negligible variation even after SOD thermal treatment.

Fig. 3 shows the XRD results of the CNFs for a wide range of angles. These are necessary to investigate the overall CNF structural properties and alloy formation during SOD thermal treatment. All the CNFs presented near-identical XRD spectra consisting of two broad peaks at 23.9° and 43.3°, corresponding to the amorphous and graphite carbon peaks, respectively.[28] No additional diffraction peaks were detected after SOD thermal treatment, even at a high temperature of 800 °C. This indicates that no other chemical species (such as carbon oxide, phosphorus oxide, or other impurities) form during SOD thermal treatment.

Fig. 4 shows CNF micro-structural investigations based on TEM and TEM-EDS measurements. Fig. 4(a) and (b) show the TEM images for conventional CNFs and CNF-SOD800, respectively. The results show that there is no significant difference in the CNF diameter after SOD thermal treatment. The

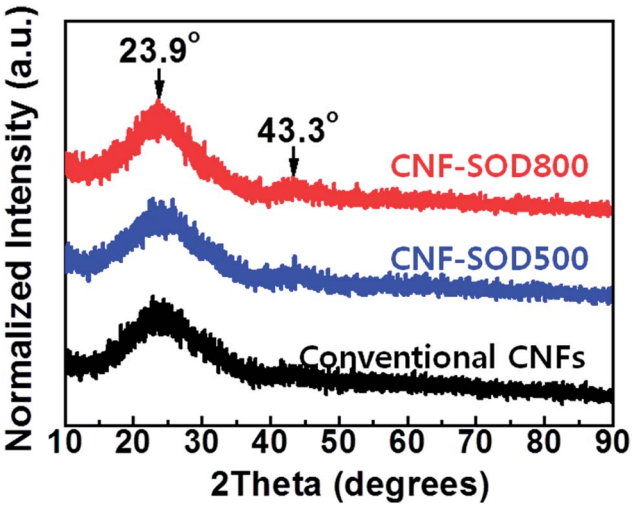

Fig. 3 Normalized θ–2θ XRD patterns for as-synthesized CNF and SOD-treated CNFs at 500 °C and 800 °C.

conventional CNFs show a dense and homogeneous morphology, while that of CNF-SOD800 is inhomogeneous and consists of ellipsoidal white regions in a dark matrix [Fig. 4(b)]. The ellipsoidal white regions, with size ranging between 20 and 40 nm, correspond to the pores formed during SOD thermal treatment. The ellipsoidal shape of the pores is formed due to the combination of the oxygen atoms in the P_2O_5 substrate and the carbon atoms in the carbon nanofibers. Fig. 4(c) shows the elemental mapping of C, O, and P taken from CNF-SOD800, and indicates that the CNF consists mainly of elemental C and O. It should be noted that CNF-SOD800 contains uniformly distributed elemental P, and there was no preferential gathering of P atoms to form P-related alloys or precipitates in the CNFs during the SOD treatment.

To investigate the formation of pores during SOD treatment, we estimated the specific surface areas and total pore volumes of CNFs from BET measurements, as summarized in Fig. 5. Both the CNF specific surface area and total pore volume increased with an increase in the SOD thermal treatment. The specific surface area of CNF-SOD800 increased by approximately 1.47 times when compared to that of conventional CNFs. This increase would be due to the increase in the total pore volume. From the adsorption and desorption measurement, more information about the CNFs was

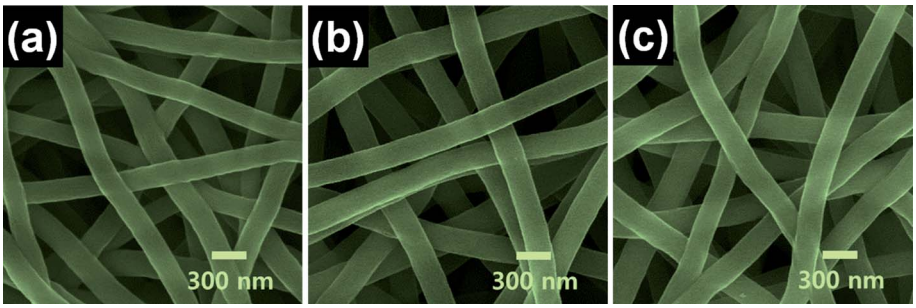

Fig. 2 FESEM images for (a) conventional CNFs, (b) CNF-SOD500, and (c) CNF-SOD800.

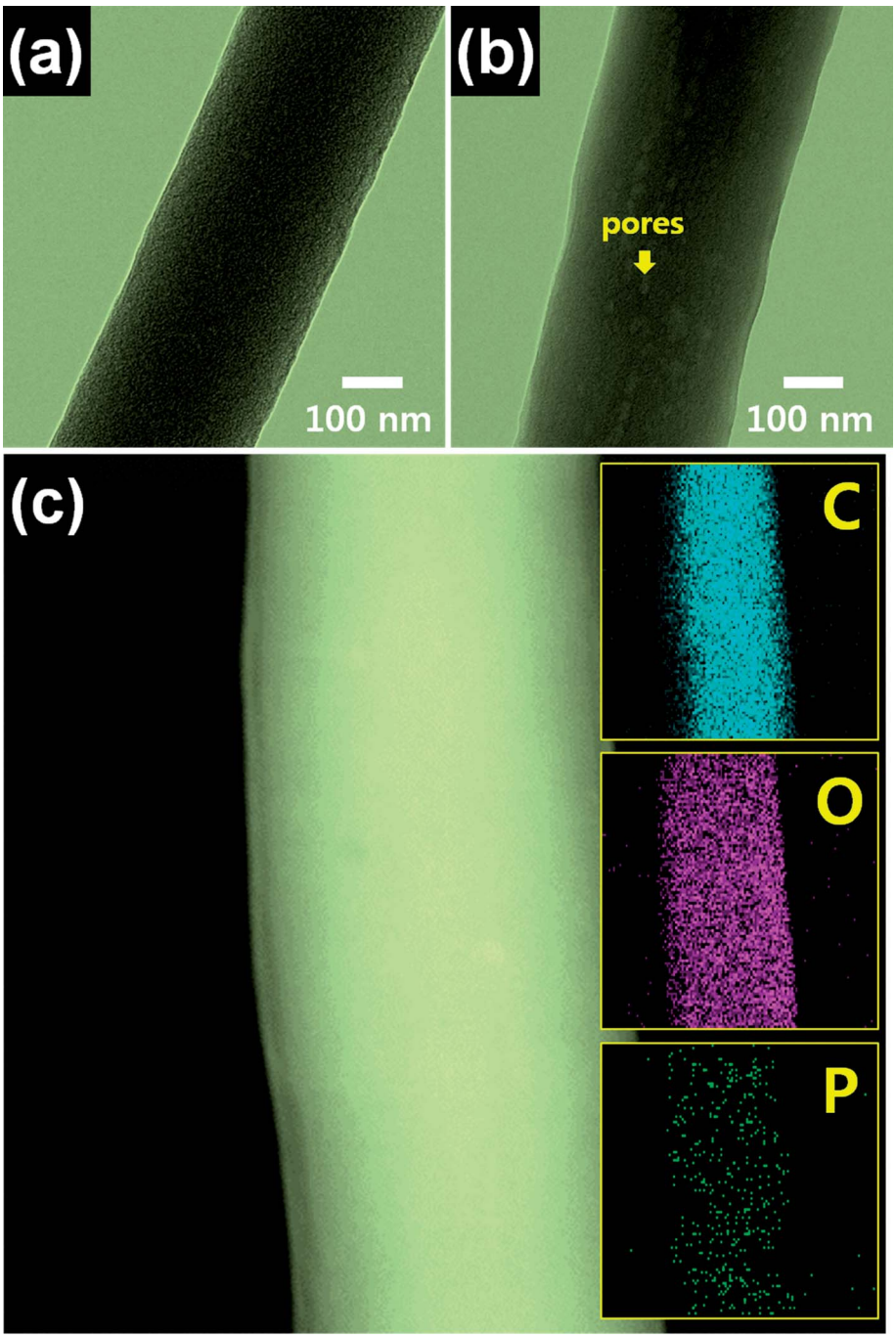

Fig. 4 TEM images for (a) conventional CNFs and (b) CNF-SOD800. (c) Elemental mapping of C, O, and P for CNF-SOD800.

obtained (see Fig. S1 in ESI† for more details). And the P incorporated CNFs showed reduced ratio of mesopore to micropore compared with the conventional CNF. It should be noted that this ratio do not imply the absolute content of the mesopore is reduced in the SOD treated CNFs because the total volume of pore has been increased for the SOD treated CNFs. This result is consistent with the TEM microstructural investigations, as shown in Fig. 4(a) and (b). The formation of pores is caused by the oxygen atoms in the P_2O_5 substrate. The oxygen atoms of the P_2O_5 substrate combine with carbon in CNFs, which then undergo sublimation to form CO_2 gas. This indicates that the thermal treatment is effective in increasing the surface area and pore volume in CNFs. The enlarged pore-containing specific surface area in the CNFs has been known to enhance the capacitance by enlarging the area for electrochemical reactions. Hereafter, we discuss this effect on the electrochemical performance in relation to the surface chemical states.

Fig. 6(a–c) show the XPS spectra of the O 1s peaks for conventional CNFs, CNF-SOD500, and CNF-SOD800, respectively.

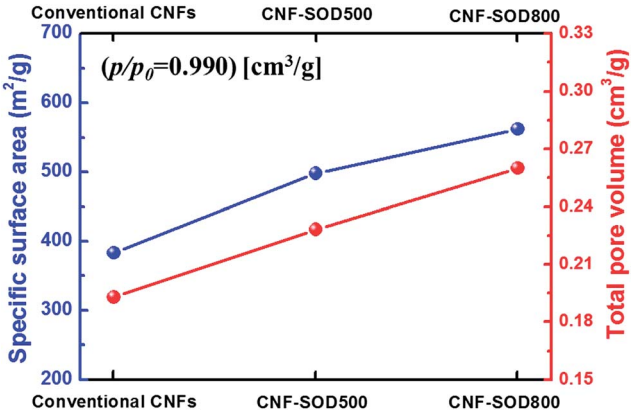

Fig. 5 Specific surface area and total pore volume for the CNFs measured by the BET method.

These can be applied to investigate the surface chemical bonding states of the CNFs. The O 1s spectrum of conventional CNFs can be deconvoluted into triple subpeaks that correspond to C–O groups (~532.6 eV), hydroxyl groups (533.6 eV), and carboxylic groups (535.0 eV), respectively. This is a typical feature for the XPS results of CNFs fabricated by an electrospinning method.[29–31] In contrast, the O 1s spectra for CNF-SOD500 and CNF-SOD800 can be decomposed into four regions that correspond to the phosphate groups (531.0 eV), C–O groups (532.5 eV), hydroxyl groups (533.6 eV), and carboxylic groups (535.0 eV), respectively.[32,33] It should be noted that the phosphate groups are found in the SOD-treated CNFs formed from the incorporation of elemental P during the SOD process. Generally, P has been known to form compounds with three, four, or five coordination, depending on the environment. The P atom replaces the two edge carbon atoms and forms phosphate and hydroxyl groups.[34–36] Table 1 summarizes the concentrations of the functional groups in each sample. The peaks from the phosphate and hydroxyl groups of CNF-SOD800 showed a higher intensity than those of CNF-SOD500. This indicates that a larger SOD treatment temperature enhances the incorporation of P atoms and the formation of hydroxyl groups. Generally, functional groups, such as phosphate and hydroxyl groups, have been known to play a critical role in improving the electrochemical properties in the CNFs. This is because they can increase the polarization and wettability of the working-ions in the electrolytes, when they are used as an electrode in electrochemical capacitors.[37–39] Therefore, we confirmed the formation of phosphate and hydroxyl groups on the CNFs by this SOD process. Based on the XPS results, we have suggested a mechanism for the surface chemical states, after SOD treatment, as shown in Fig. 6(d). The phosphate and hydroxyl groups are formed on the CNF surface as a result of P incorporation. The P atoms show three, four, and five coordination in the compounds formed. These P atoms replace the two edge carbon atoms in the graphite structure of the CNFs. The electrical conductivity of the CNFs was measured by the electrochemical impedance spectroscopy (EIS). And the resistance of CNFs was reduced after the SOD treatment and the CNF-SOD800 showed the smallest resistance (see Fig. S2 in ESI† for more details). And these would be attributed from the P incorporation into the CNFs to increase the conductivity. Thus, we synthesized the P-incorporated CNFs successfully by combining the unique methods of electrospinning and SOD procedures.

Fig. 7(a) shows the CV curves of conventional CNFs, CNF-SOD500, and CNF-SOD800. The CV measurements were attained using a potentiostat/galvanostat at a scan rate of 10 mV s^{-1}, and a potential range between 0.0 and 1.0 V in 6 M KOH solution. The CV curves for all samples showed a quasi-rectangular shape in the measured potential region, indicating

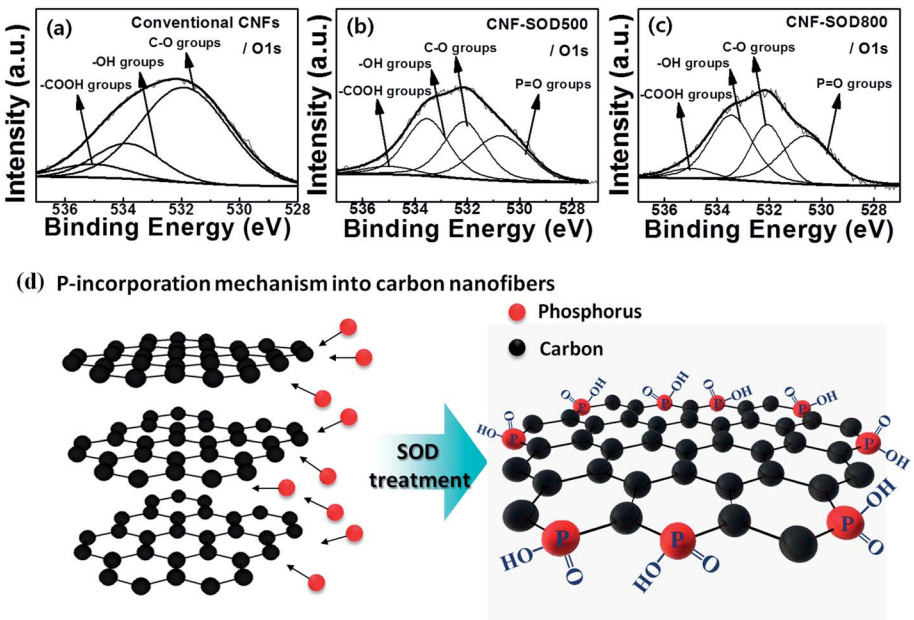

Fig. 6 XPS spectra of O 1s for (a) conventional CNFs, (b) CNF-SOD500, and (c) CNF-SOD800. The elementary XPS spectra shown by solid lines were obtained by deconvolution. (d) Schematics for the P-incorporation mechanism into CNFs by the SOD method.

Table 1 Summary of the XPS signals for each surface functional group in the CNFs

	–COOH (535.0 eV)	–OH (533.6 eV)	C–O (532.3 eV)	P=O (531.0 eV)
Samples	Concentration (%)	Concentration (%)	Concentration (%)	Concentration (%)
Conventional CNFs	8.06	20.07	71.87	—
CNF-SOD500	5.28	33.28	32.15	29.29
CNF-SOD800	5.21	38.11	23.41	33.27

a capacitive behaviour that mainly arises from the charge and discharge of the electric double layer. The SOD-treated CNFs showed larger quasi-rectangular curves than those of conventional CNFs. Also, the quasi-rectangular curve becomes larger with an increase in the SOD treatment temperature. This is due to the increased specific surface area and the effect of the functional groups. The CV curve for CNF-SOD800 showed the largest quasi-rectangular curve area, and this indicates that CNF-SOD800 has excellent capacitive properties owing to a high specific surface area and its functional groups. Fig. 7(b) shows the specific capacitance of conventional CNFs, CNF-SOD500, and CNF-SOD800. The specific capacitance can be calculated from the following equation:[40]

$$C_{sp} = 4I/(m\mathrm{d}V/\mathrm{d}t) \quad (1)$$

where C_{sp} is the specific capacitance, t is the discharging time (s), $\mathrm{d}V/\mathrm{d}t$ is the scan rate, m is the total mass of the active material (g), and I is the current (A). The specific capacitances of conventional CNFs, CNF-SOD500, and CNF-SOD800 at a current density of 0.1 A g^{-1} are 76 F g^{-1}, 160 F g^{-1}, and 188 F g^{-1}, respectively. The discharge time was estimated from the galvanostatic charge–discharge curves obtained conventional CNFs, CNF-SOD500, and CNF-SOD800 using symmetric two-electrode cells in 6 M KOH at 1 A g^{-1}. And the discharge time for conventional CNFs, CNF-SOD500, and CNF-SOD800 were 32, 61, and 71 s, respectively (see Fig. S3 in ESI† for more details). For all current densities, CNF-SOD800 showed the largest specific capacitance. This is because CNF-SOD800 has a high specific surface area and a large amount of beneficial functional groups, such as phosphate and hydroxyl groups, as shown in Fig. 6(c). Functional groups containing oxygen atoms can improve the polarization and wettability of the electrolyte.[41] In addition, on increasing the current density, the specific capacitance of the ECs is reduced due to a decrease in the ion diffusion time during the charge/discharge processes. However, CNF-SOD800 exhibited an excellent high-rate specific capacitance performance of 138 F g^{-1}, even at a current density of 2.6 A g^{-1}, and the capacitance was maintained at 73% of the initial value. These results originate from the increased oxygen-containing

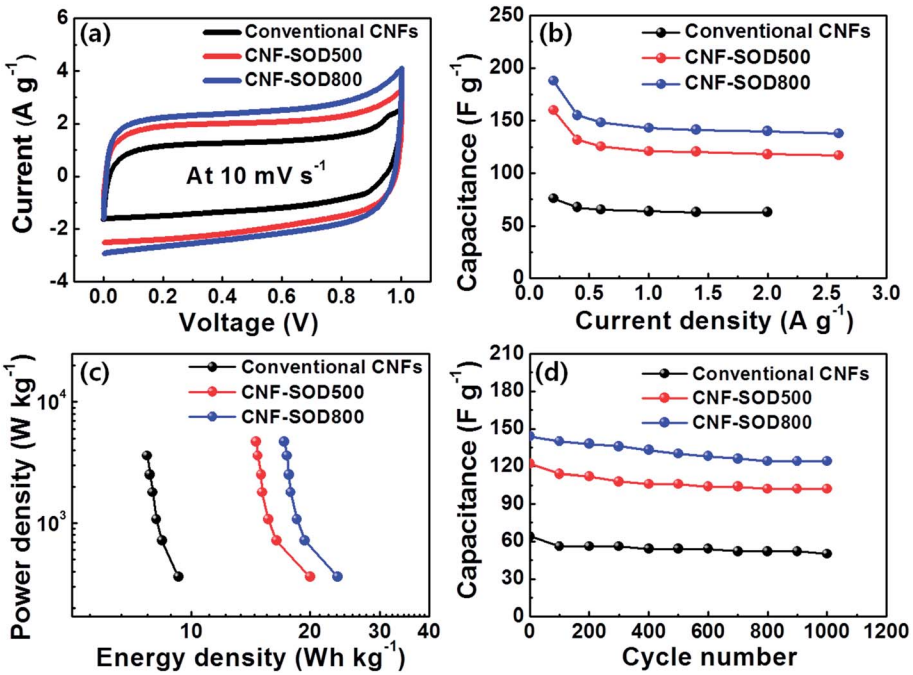

Fig. 7 (a) CV measurements obtained for the electrode of conventional CNFs, CNF-SOD500, and CNF-SOD800 at a scan rate of 10 mV s^{-1} in the voltage range 0.0–1.0 V. (b) Specific capacitance data obtained for the ECs with CNF electrodes at current densities between 0.2 and 2.6 A g^{-1}. (c) Ragone plot data obtained for the ECs with CNF electrodes in a power density range of 360 and 3600 W kg^{-1}. (d) Cycling stability measurements obtained for the ECs with CNF electrodes at a current density of 1.0 A g^{-1} for up to 1000 cycles.

functional groups that improve the accessibility of the ions, even at a high current density. For more analysis about the capacitance, the electrochemical performance was measured by using three-electrode system. In the three-electrode system, the SOD treated CNFs exhibited electric double layer capacitance and pseudocapacitance behaviours owing to the surface functional groups (see Fig. S4 in ESI† for more details). Fig. 7(c) is a Ragone plot of the EC energy density (E, W h kg^{-1}) *versus* power density (P, W kg^{-1}). The EC energy density and power density values were calculated from the following equations based on the galvanostatic charge/discharge measurements:[40]

$$E = \frac{C_{sp} V^2}{8} \quad (2)$$

$$P = \frac{E}{dt} \quad (3)$$

where V is the discharge voltage (V) and dt is the total discharge time. Typically, the Ragone plot shows that the energy density decreases with an increase in the power density. The energy density of the conventional CNFs ranges between 7.7 and 9.3 W h kg^{-1} in a power density range between 360 and 3600 W kg^{-1}. The energy and power densities of the ECs were greatly enhanced after SOD treatment, and with an increase in the SOD treatment temperature. The energy density of CNF-SOD800 was between 2.2 and 2.5 times larger, and the power density was 1.2 times larger, when compared to conventional CNFs. This enhancement originates from the combined beneficial effects of an enlarged surface area and the modification of the chemical functional groups on the CNFs during the SOD treatment. Fig. 7(d) shows the cycling stabilities of ECs fabricated from various CNFs. Thus, the EC with conventional CNFs had a cycling ability of 50 F g^{-1} with a retention of 78% after 1000 cycles, while that with CNF-SOD800 exhibited the largest capacitance value (124 F g^{-1}) with a retention of 86% even after 1000 cycles at 1 A g^{-1}. In this way, the SOD treatment induced P incorporation also enhances the cycling stabilities of the ECs. Therefore, the enhancement of the electrochemical properties of the CNFs after SOD treatment can be explained by two main effects: one is the enlargement of the specific surface area to increase the reaction area between the electrode and the electrolyte, and the other is the formation of beneficial functional groups, such as phosphate and hydroxyl groups, to improve the CNF polarization and wettability of the electrolyte. The use of the SOD method can provide beneficial effects for the incorporation of foreign elements into nanostructures because they have low diffusion activation energy and all spatial diffusion directions. This enables the effective incorporation of dopants into nanostructures with complicated shapes, even at low temperatures.

4. Conclusion

We fabricated P-incorporated CNFs by combining electrospinning and SOD methods. The structural investigations by FESEM and XRD results showed that there was negligible variation in the CNF shapes, and no formation of chemical species, such as carbon oxide, phosphorus oxide, or other impurities, even after SOD thermal treatment. Microstructural investigations by TEM and EDS showed the formation of pores with sizes ranging between 20 and 40 nm, and uniformly distributed elemental P for the CNFs after SOD thermal treatment. The specific surface areas and total pore volumes of the CNFs greatly increased after both simple heat and SOD treatment. Notably, the SOD-treated CNFs contained many beneficial functional groups, such as phosphate and hydroxyl groups. Because of these two beneficial effects, the ECs with SOD-treated CNF electrodes showed excellent electrochemical properties, such as enhancement of the power density, energy density, specific capacitance, and cycling stability of ECs. Therefore, the proposed SOD method can provide beneficial effects for incorporation of foreign elements into carbon-based nanostructures because they have low diffusion activation energy and all spatial diffusion directions. These properties enable effective incorporation of dopants into nanostructures with complicated shapes, even at low temperatures.

Acknowledgements

The authors thank Mr Gwang-Hee Nam (Yeungnam University) for assistance with the experiments. This research was supported by Basic Science Research Program (No. NRF-2015R1A1A1A05001252) and (No. NRF-2014R1A2A1A11054154) through the National Research Foundation of Korea funded by the Ministry of Science, ICT and Future Planning.

References

1 N. Akizuki, S. Aota, S. Mouri, K. Matsuda and Y. Miyauchi, *Nat. Commun.*, 2015, **6**, 8920.
2 G. Zheng, S. W. Lee, Z. Liang, H. W. Lee, K. Yan, H. Yao, H. Wang, W. Li, S. Chu and Y. Cui, *Nat. Nanotechnol.*, 2014, **9**, 618.
3 B. K. Min, S. K. Kim, S. J. Kim, S. H. Kim, M. A. Kang, C. Y. Park, W. Song, S. Myung, J. Lim and K. S. An, *Sci. Rep.*, 2015, **5**, 16001.
4 V. Veeramani, R. Madhu, S. M. Chen, B. S. Lou, J. Palanisamy and V. S. Vasantha, *Sci. Rep.*, 2015, **5**, 10141.
5 G. A. Ferrero, A. B. Fuertes and M. Sevilla, *Sci. Rep.*, 2015, **5**, 16618.
6 X. Xiao, T. Beechem, D. R. Wheeler, D. B. Burckel and R. Polsky, *Nanoscale*, 2014, **6**, 2629–2633.
7 L. Yan, F. Zhao, S. Li, Z. Hu and Y. Zhao, *Nanoscale*, 2011, **3**, 362–382.
8 H. Sun, X. He, J. Ren, J. Li, C. Jiang and C. Wan, *Electrochim. Acta*, 2007, **52**, 4312–4316.
9 M. Zhi, S. Liu, Z. Hong and N. Wu, *RSC Adv.*, 2014, **4**, 43619–43623.
10 L. Zhang, L. Han, S. Liu, C. Zhang and S. Liu, *RSC Adv.*, 2015, **5**, 107313–107317.
11 J. B. Lee, S. Y. Jeong, W. J. Moon, T. Y. Seong and H. J. Ahn, *J. Alloys Compd.*, 2011, **509**, 4336–4340.
12 Z. Yang, G. Du, Z. Guo, X. Yu, S. Li, Z. Chen, P. Zhang and H. Liu, *Nanoscale*, 2010, **2**, 1011–1017.

13 S. U. Kim and K. H. Lee, *Chem. Phys. Lett.*, 2004, **400**, 253–257.
14 G. H. An and H. J. Ahn, *Electrochem. Solid-State Lett.*, 2013, **2**, M33–M36.
15 H. Zhang, X. Zhang, X. Sun and Y. Ma, *Sci. Rep.*, 2013, **3**, 3534.
16 G. H. An and H. J. Ahn, *Carbon*, 2013, **65**, 87–96.
17 F. Zhang, C. Yuan, J. Zhu, J. Wang, X. Zhang and X. W. Lou, *Adv. Funct. Mater.*, 2013, **23**, 3909–3915.
18 L. F. Chen, Z. H. Huang, H. W. Liang, H. L. Gao and S. H. Yu, *Adv. Funct. Mater.*, 2014, **24**, 5104–5111.
19 Y. J. Lee, D. G. Kim and H. J. Ahn, *Electrochem. Solid-State Lett.*, 2015, **4**, M1–M4.
20 L. F. Chen, Z. H. Huang, H. W. Liang, Q. F. Guan and S. H. Yu, *Adv. Mater.*, 2013, **25**, 4746–4752.
21 D. W. Wang, F. Li, Z. G. Chen, G. Q. Lu and H. M. Cheng, *Chem. Mater.*, 2008, **20**, 7195–7200.
22 Y. Wen, B. Wang, C. Huang, L. Wang and D. H. Jurcakova, *Chem.–Eur. J.*, 2015, **21**, 80–85.
23 M. Jamil, J. Mantey, E. U. Onyegam, G. D. Carpenter, E. Tutuc and S. K. Banerjee, *IEEE Electron Device Lett.*, 2011, **32**, 1203.
24 J. Jourdan, Y. Veschetti, S. Dubois, T. Desrues and R. Monna, *Prog. Photovoltaics*, 2008, **16**, 379–387.
25 J. Oh, K. Im, C. G. Ahn, J. H. Yang, W. J. Cho, S. Lee and K. Park, *Mater. Sci. Eng., B*, 2004, **110**, 185–189.
26 D. Mathiot, A. Lachiq, A. Slaoui, S. Noel, J. C. Muller and C. Dubois, *Mater. Sci. Semicond. Process.*, 1998, **1**, 231–236.
27 J. I. Sohn, Y. I. Jung, S. H. Baek, S. Cha, J. E. Jang, C.-H. Cho, J. H. Kim, J. M. Kim and I. K. Park, *Nanoscale*, 2014, **6**, 2046.
28 M. J. Kim, J. T. Yeon, K. Hong, S. I. Lee, N. S. Choi and S. S. Kim, *Bull. Korean Chem. Soc.*, 2013, **34**, 2029.
29 A. J. Plomp, D. S. Su, K. P. de Jong and J. H. Bitter, *J. Phys. Chem. C*, 2009, **113**, 9865–9869.
30 D. Rosenthal, M. Ruta, R. Schlogl and L. Kiwi-Minsker, *Carbon*, 2010, **48**, 1835–1843.
31 J. H. Zhou, Z. J. Sui, J. Zhu, P. Li, D. Chen, Y. C. Dai and W. K. Yuan, *Carbon*, 2007, **45**, 785–796.
32 X. Yan, Y. Liu, X. Fan, X. Jia, Y. Yu and X. Yang, *J. Power Sources*, 2014, **248**, 745–751.
33 C. Wang, Y. Zhou, L. Sun, Q. Zhao, X. Zhang, P. Wan and J. Qiu, *J. Phys. Chem. C*, 2013, **117**, 14912–14919.
34 J. Laine, A. Calafat and M. Labady, *Carbon*, 1989, **27**, 191–195.
35 A. M. Puziy, O. I. Poddubnaya, R. P. Socha, J. Gurgul and M. Wisniewski, *Carbon*, 2008, **46**, 2113–2123.
36 S. G. Oh and N. M. Rodriguez, *J. Mater. Res.*, 1993, **8**, 2879.
37 M. Ishikawa, A. Sakamoto, M. Morita, Y. Matsuda and K. Ishida, *J. Power Sources*, 1996, **60**, 233–238.
38 L. F. Chen, X. D. Zhang, H. W. Liang, M. Kong, Q. F. Guan, P. Chen, Z. Y. Wu and S. H. Yu, *ACS Nano*, 2012, **6**, 7092–7102.
39 G. H. An and H. J. Ahn, *J. Electroanal. Chem.*, 2015, **744**, 32–36.
40 M. Liu, W. W. Tjiu, J. Pan, C. Zhang, W. Gao and T. Liu, *Nanoscale*, 2014, **6**, 4233–4242.
41 E. Cruz-Silva, F. Lopez-Urias, E. Munoz-Sandoval, B. G. Sumpter, H. Terrones, J. C. Charlier, V. Meunier and M. Terrones, *Nanoscale*, 2011, **3**, 1008–1013.